



CHALMERS
UNIVERSITY OF TECHNOLOGY

A fiber-optic nanoplasmonic hydrogen sensor: Via pattern-transfer of nanofabricated PdAu alloy nanostructures

Downloaded from: <https://research.chalmers.se>, 2026-04-16 04:40 UTC

Citation for the original published paper (version of record):

Nugroho, F., Eklund, R., Nilsson, S. et al (2018). A fiber-optic nanoplasmonic hydrogen sensor: Via pattern-transfer of nanofabricated PdAu alloy nanostructures. *Nanoscale*, 10(44): 20533-20539. <http://dx.doi.org/10.1039/c8nr03751e>

N.B. When citing this work, cite the original published paper.



Cite this: *Nanoscale*, 2018, **10**, 20533

Received 9th May 2018,
 Accepted 21st October 2018
 DOI: 10.1039/c8nr03751e

rsc.li/nanoscale

A fiber-optic nanoplasmonic hydrogen sensor via pattern-transfer of nanofabricated PdAu alloy nanostructures†

Ferry Anggoro Ardy Nugroho,¹ * Robin Eklund, Sara Nilsson¹ and Christoph Langhammer¹ *

We demonstrate the transfer of arrays of nanofabricated noble metal and alloy nanostructures obtained by high-temperature annealing on a flat parent support onto optical fibers, to create a hysteresis-free fiber optic nanoplasmonic hydrogen sensor. This work enables the integration of complex nanofabricated structures and their arrangements in tailored arrays with fiber optics to realize optical sensors, which will find application in a wide range of disciplines.

Fiber optic sensors exhibit unique features such as cheap mass production potential, multichannel distributive and remote readout capability, small footprint and immunity to electromagnetic interference. Thus, they are already today finding application in multiple fields ranging from bio- to industrial process monitoring^{1–3} and from gas- to chemosensing.^{4,5} The sensing activity in a fiber optic sensor is typically mediated by either an optical property change of the measured analyte itself (*e.g.* a refractive index change), indirectly through surface-bound transducing agents such as fluorescent molecules,^{2,6} or by thin noble metal films grown onto the fiber, which enable surface plasmon resonance (SPR) detection.^{7–9} More recently, driven by the great promise of nanoplasmonic sensors¹⁰ that rely on nanoparticle signal transducers, attempts to deposit plasmonic nanoparticles onto fibers by self-assembly of colloidal nanoparticles^{11–13} and, to a much smaller extent, by dewetting of a sputtered thin film^{14,15} have also been reported. However, these solutions are so far restricted to small (<50 nm) and single-element Au (and Ag¹⁶) nanoparticles due to inherent limitations of colloidal synthesis to produce monodisperse large nanoparticles, in particular when it comes to more complex materials like alloys.^{17–19} Moreover, self-assembly provides little to no control of the nanoparticle surface density on the fiber. These limitations are

unfortunate because integration of nanoplasmonic sensors with optical fiber technology has significant potential to bring the field closer to application in practical sensor technology.

To enable such a breakthrough, finding new ways to grow or deposit complex nanostructures, tailored in terms of size, shape and composition, onto optical fibers is necessary. To this end, such structures are readily available *via* nanolithography-based fabrication techniques where methods like electron-beam lithography and colloidal lithography have been demonstrated to enable the crafting of myriads of (complex) nanostructures with excellent control of the aforementioned key parameters.^{20–23} However, these methods typically require flat supports and, consequently, they are incompatible with optical fibers.

In response, in this communication we present a solution for the deposition of nanofabricated noble metal alloy nanostructure arrays onto optical fibers by further developing a pattern transfer method recently reported by Lodewijks *et al.*²⁴ Specifically, we transfer PdAu alloy nanodisk arrays, fabricated by Hole-Mask Colloidal Lithography (HCL) on a flat support²⁵ compatible with high-temperature annealing at 500 °C, onto optical fibers. In this way, we enable a fiber optic nanoplasmonic hydrogen sensor that features hysteresis-free and fast response, for which the high-temperature treatment necessary to induce alloy formation can be carried out *prior* to the pattern transfer, thus entirely eliminating thermal damage to the fiber. Furthermore, the use of nanofabricated nanoparticle arrays with controlled composition provides access to design rules that enable the tailoring and maximizing of the sensor limit of detection by engineering nanoparticle size and shape and thus their plasmonic response,²⁶ yielding performance superior to thin film solutions.^{27,28}

We chose this particular application to demonstrate our nanopattern transfer method because a fiber optic platform is very attractive for hydrogen detection due to its effective remote readout that reduces the risk of spark generation at flammable hydrogen concentrations (*i.e.* 4–75 vol% H₂), as well as due to its small geometrical footprint and mass-pro-

Department of Physics, Chalmers University of Technology, 412 96 Göteborg, Sweden. E-mail: ferryn@chalmers.se, clangham@chalmers.se

† Electronic supplementary information (ESI) available. See DOI: 10.1039/c8nr03751e



duction potential. To this end, fiber optic hydrogen sensors employing diverse sensing mechanisms such as evanescent field intensity,^{29–31} reflection,^{32–35} fiber-grating,^{36–38} interferometry^{39,40} and SPR^{41–43} have been reported. The majority of these sensors employ Pd (and its alloys^{33,40,44}) as the active material since it enables effective hydrogen detection with high selectivity under ambient conditions as only hydrogen can induce the phase transformation to a hydride phase that gives rise to the optical contrast used as the readout.⁴⁵ This contrast is induced by the absorption of hydrogen in interstitial lattice positions in the Pd host, which both alters the electronic structure, and the volume due to lattice expansion.^{46,47} However, all of these sensors, with a few exceptions,⁴⁰ employ thin Pd films as active material, and thus they are prone to durability issues due to cracking and peeling of the films. Moreover, readouts other than evanescent field and reflectivity change often require complicated fabrication and setups.⁴

Also, the use of neat Pd as transducer material as such has significant shortcomings. For example, due to an energy barrier created by lattice strain during phase transformation to the hydride, hysteresis between hydrogen absorption and desorption is observed⁴⁸ and hampers sensor accuracy and dynamic range. The former is adversely affected since the response will depend on sensor history, and readout may thus be ambiguous.^{48,49} The latter is limited in the sense that Pd features a large response only in a very narrow hydrogen pressure range, *i.e.* around the phase transformation in the $\alpha + \beta$ phase coexistence region.^{48,49} Finally, it is also predicted that thin films are inferior as hydrogen sensor transducers since nanoparticles have the potential to provide faster

response due to shorter diffusion paths.⁵⁰ Therefore, realizing a nanoplasmonic fiber-optic hydrogen sensor, where nanoparticles with tunable sensitivity *via* shape and size engineering, as well as with tailored chemical composition,²⁶ act as signal transducers, is highly desirable. Specifically, Pd-based coinage-metal alloys are attractive because they feature faster hysteresis-free response and higher resistance towards poisoning and deactivation by species like CO and NO₂ compared to neat Pd.^{44,51–53}

To achieve such an optical nanoplasmonic Pd-alloy based fiber-optic hydrogen sensor, we have developed the specific sequence of nanofabrication steps outlined in Fig. 1 to transfer an amorphous array of alloy nanostructures made by HCL^{22,25} on a flat support, to an optical fiber. The key component enabling this process is the presence of a sacrificial Cr-layer and a thin C transfer layer that provide the means for lifting-off and transferring the nanostructures from the flat to the fiber support. Hence, these two layers are first deposited onto the flat support (here borofloat glass) by electron beam evaporation of a 100 nm thick Cr-film, followed by 10 nm of C (Fig. 1a). In the next step, the nanoparticles are defined by HCL nanofabrication onto the Cr/C sandwich support, followed by the layer-by-layer deposition of Au and Pd through the mask to produce a square centimeter quasi-random array of nanodisks with 170 nm average diameter, and a thickness of 25 nm (Fig. S1†). After lifting-off the mask, we annealed the sample at 500 °C for 24 h under H₂ flow to induce the formation of a homogeneous PdAu alloy comprised of 75 at% Pd and 25 at% Au, as predefined by the respective thickness of the evaporated layers.²⁵ We chose this particular alloy compo-

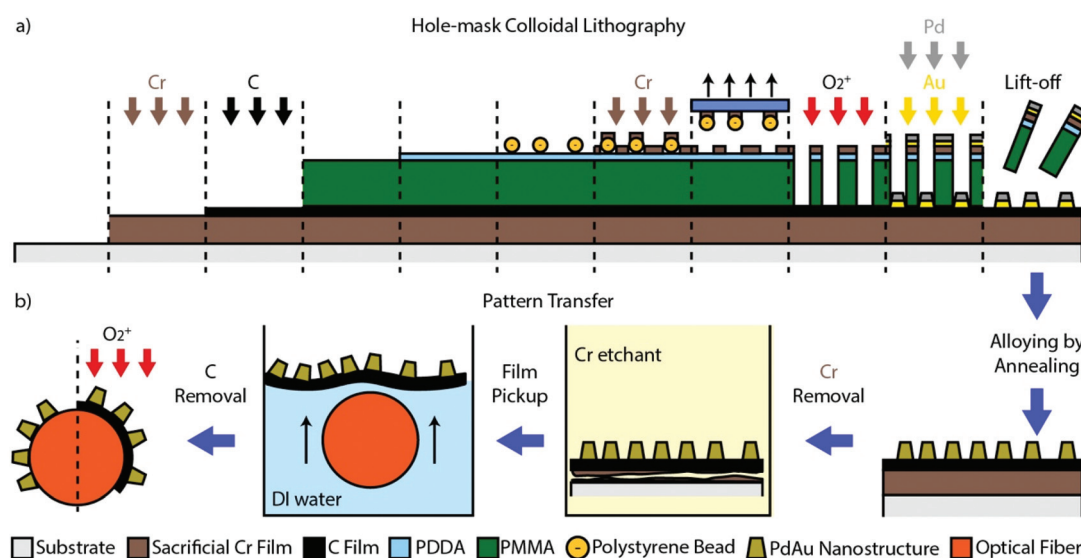


Fig. 1 (a) The steps of the growth of the sacrificial Cr-layer and the C-pattern-transfer-layer, followed by the Hole-mask Colloidal Lithography (HCL)^{22,25} nanofabrication of the PdAu alloy nanodisk array. (b) The sequence of the pattern transfer steps to the optical fiber. Once the Cr-layer is removed by wet etching, the C-layer with the nanoparticles is detached but still resides on the substrate. The substrate can therefore be used to pick up the C-layer and move it into deionized water. Due to the hydrophobicity of the C-layer, it will then readily float up to the water–air interface, providing access for the optical fiber to pick it up and complete the transfer process. Once dried, oxygen plasma is utilized to remove the C-layer, leaving only the nanodisk array on the fiber. Note that the schematic is not drawn to scale.



sition as it enables the complete suppression of hysteresis between hydrogen absorption and desorption, which is critical in a hydrogen sensing application.^{28,52} Mechanistically, hysteresis is suppressed by pre-straining the Pd lattice by the Au (or other atoms with different atomic radius than Pd, *e.g.*, Ag, Cu or Ni^{25,44,52–54}) and the concurrent lowering of the critical temperature for the formation of the hydride phase. Furthermore, the high-temperature annealing step is also necessary to increase the mechanical stability of the C-layer, to enable the pattern transfer.²⁴

After completion of the nanofabrication and alloy formation, the pattern transfer to the optical fiber can be initiated and executed following the steps depicted in Fig. 1b (see also Fig. S3† for photographs). First, the Cr sacrificial layer is dissolved by immersing the sample in a Cr-etchant solution, in this way detaching the C-film with the alloy nanoparticle array from the glass substrate. Once the Cr-layer is completely removed (as indicated by a distinct color change of the sample, see Fig. S3†) the C film can be picked up by the glass substrate and moved into deionized water. Due to the hydrophobic nature of the C film, it readily floats at the water–air interface. This makes it possible in the next step to “pick it up” by careful immersion of the desired part of the optical fiber and in this way transfer the nanofabricated pattern onto it (or essentially any other support of interest²⁴). In this process, the very thin, flexible, and yet mechanically stable C film support enables the conformal transfer of the pattern onto the entire fiber (*i.e.* around it), if the correct size of the transferred pattern is prepared. After drying, as the final step, an oxygen plasma treatment is utilized to remove the C film, leaving only the array of alloyed Pd₇₅Au₂₅ nanodisks that reside on the fiber.

To evaluate the hydrogen sensing function of optical fibers decorated with a nanofabricated Pd₇₅Au₂₅ alloy nanoparticle array, we used a commercial multimode fiber with 300 μm SiO₂ core and hard fluoropolymer cladding, and we implemented the optical readout as a combination of evanescent field and reflection mode, as shown in Fig. 2a. Specifically, we transferred the Pd₇₅Au₂₅ alloy particles onto the end of a fiber, where we previously had removed the cladding (see Fig. S2† for fiber configuration and the Methods section in the ESI† for details). In this way, upon hydrogen sorption in the nanoparticles, the evanescent field of the light transported through the fiber will be modified *via* coupling to the localized surface plasmon resonance (LSPR) in the nanoparticles, whose permittivity changes proportionally to the hydrogen concentration in the environment.^{26,55,56} This, in turn, gives rise to a wavelength-dependent variation of the transmitted light intensity,^{26,55,57} which we pick up in reflection mode by growing a 300 nm thick Al mirror at the tip, as a means to reflect the light back into a spectrometer *via* a bifurcated fiber (Fig. 2a and S4†).

Fig. 2b shows an optical micrograph of such a fiber, decorated with the transferred C film and the Pd₇₅Au₂₅ alloy nanoparticle array, revealing the conformity of the coating. The same fiber is shown after the oxygen plasma treatment, which

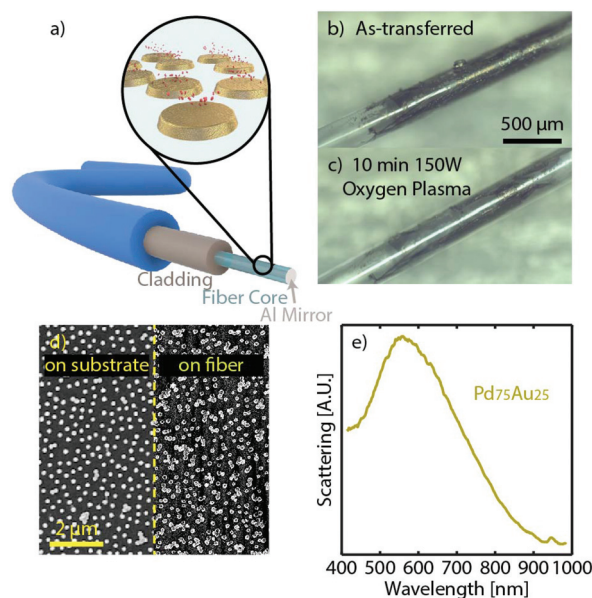


Fig. 2 (a) An artist's rendition of a fiber-optic nanoplasmonic hydrogen sensor, where a transferred array of PdAu alloy nanoparticles on the unclad portion of an optical fiber constitutes the signal transducer, *via* its permittivity changes induced by hydrogen sorption. Note that the tip of the fiber is coated with an Al mirror to enable efficient readout of the modified light propagation properties due to the hydrogenation of the nanoparticles *via* back reflection. (b) Optical micrograph of the as-transferred pattern with the C-transfer layer still in place. (c) Optical micrograph of the same fiber after 10 min oxygen plasma treatment. (d) SEM images of the Pd₇₅Au₂₅ alloy nanodisk array on the parent substrate (left) and on the optical fiber, after transfer process (right). Note that the particle arrangement is retained despite minor agglomeration. (e) Dark-field scattering spectrum of the Pd₇₅Au₂₅ alloy nanodisk array measured directly on the fiber, which reveals a distinct LSPR peak around 550 nm.

removes the C-layer and leaves behind only the Pd₇₅Au₂₅ alloy nanoparticle array (Fig. 2c), as confirmed by SEM (Fig. 2d). To this end, we note that the minor particle agglomeration seen in the SEM image will not affect the particle sensing functionality since a distinct LSPR scattering peak around 550 nm can be resolved by dark-field scattering spectroscopy (Fig. 2e).

Having successfully transferred an array of Pd₇₅Au₂₅ alloy nanoparticles onto a fiber, we now turn to assessing its hydrogen sensing functionality. For this purpose we placed the sensor in a flow reactor, which enables controlled exposure of the sample to hydrogen pulses in Ar carrier gas at a constant temperature of 30 °C, with gradually increasing hydrogen partial pressure (Fig. 3a, see also the Methods section for experimental details). At the same time, we measured the broadband optical transmission through our fiber probe in the 400–1000 nm range by employing a self-referencing scheme, that is, by defining the transmitted intensity at each wavelength as the zero baseline at the beginning of each measurement (Fig. 3b). Except at the wavelengths close to the LSPR peak of the alloy around 550 nm (in excellent agreement with the dark-field scattering spectrum in Fig. 2e), a distinct step-wise change in the optical signal appears when hydrogen is



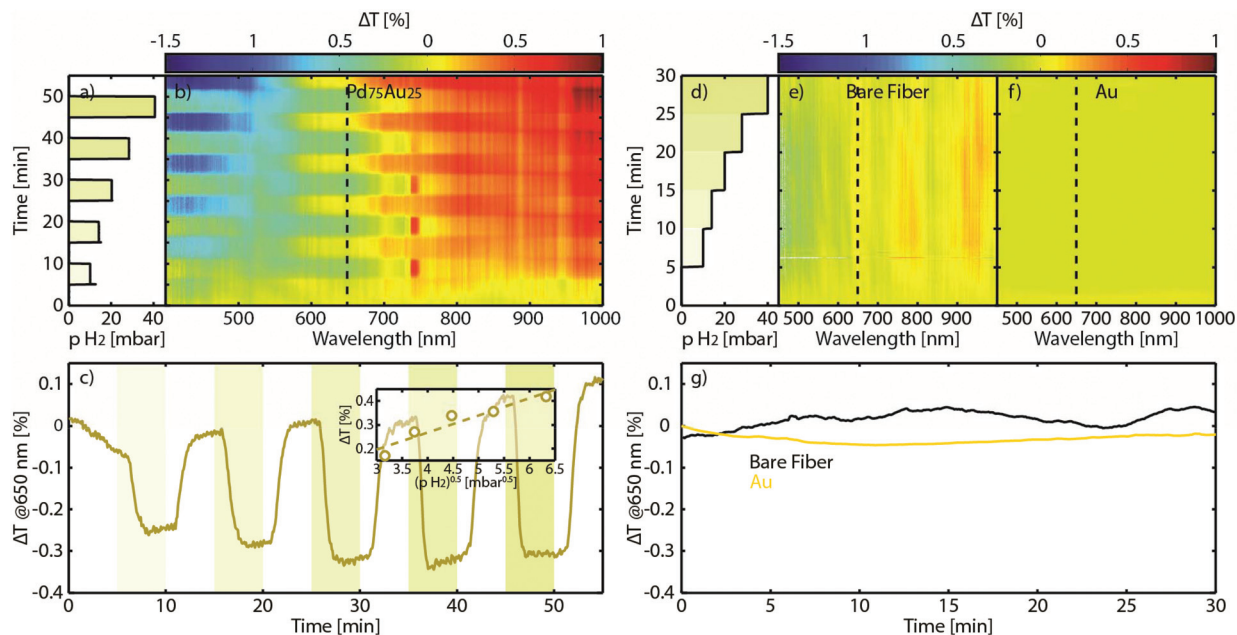


Fig. 3 (a) Depiction of the sequence of hydrogen pulses with increasing partial pressure applied to measure the Pd₇₅Au₂₅ alloy fiber optic sensor response. (b) Corresponding color-coded wavelength-resolved optical transmission contrast change ΔT of the Pd₇₅Au₂₅ alloy fiber optic sensor. The dashed line depicts the 650 nm wavelength at the inflection point of the LSPR peak. (c) Temporal response of the ΔT at 650 nm. Shaded areas mark the time where the sensor is exposed to H₂. We note a gradual baseline shift of ΔT due to minute movement of the fiber (see Methods). Inset: A linear change in ΔT as a function of the square root of the H₂ partial pressure is found, in good agreement with Sievert's law for a solid solution. (d) Depiction of the sequence of hydrogen partial pressure steps for control experiments on a blank and Au nanodisk array decorated fiber. The corresponding color-coded wavelength-resolved ΔT for (e) the bare unclad fiber and (f) the fiber decorated with an Au nanoparticle array. The dashed lines mark the 650 nm wavelength used in (g). Clearly there is no apparent response of both control samples to a variation in H₂ partial pressure.

introduced, and whose amplitude nicely scales with the H₂ partial pressure. In very good agreement with our previous work on flat sensors using a traditional nanoplasmonic sensing configuration, the highest change in optical transmission contrast, ΔT , occurs at the inflection points of the LSPR peak.^{53,58,59} Hence, peak-tracking is not necessary and monochromatic readout using cheap components like LEDs and photodiodes is readily enabled. To this end, plotting the ΔT at the 650 nm inflection point as a function of the square root of the H₂ partial pressure in the feed reveals a linear relation obeying Sievert's law for a hydrogen solid solution in the host (Fig. 3c). This feature is in very good agreement with our previous studies of PdAu alloy hydrogen sensors on traditional flat supports,^{26,53} confirming that after the pattern transfer all sensor and material-related functionalities are retained.

To further corroborate these results, we also performed measurements on two negative control samples: a bare optical fiber with the cladding removed, and a fiber onto which we transferred an array of pure Au nanodisks with similar dimensions as the PdAu alloy structures. Since Au does not absorb hydrogen itself but acts as sensitive probe for its environment *via* LSPR,¹⁰ it provides insights into whether either the fiber itself or, *e.g.*, C residues from the pattern transfer are responsible for the observed response to hydrogen. The wavelength-resolved ΔT change upon a step-wise increase of the H₂ partial

pressure from 0 to 40 mbar (Fig. 3d) is shown in Fig. 3e for the bare fiber and in Fig. 3f for the Au nanoparticle control, respectively. Clearly there is no discernible response in both control measurements, as further highlighted in Fig. 3g.

As the final step of our study, we first characterized the hydrogen sorption properties, from a materials science perspective, of the transferred PdAu alloy nanoparticle array, as well as of a pure Pd analogue for comparison. Specifically, we measured the optical pressure-composition isotherms of both systems directly on the fibers at 30 °C, using the monochromatic ΔT at 650 nm as the readout (Fig. 4a). For the neat Pd, an isotherm characterized by the wide $\alpha + \beta$ phase coexistence region ("plateau") reveals itself, together with the expected hysteresis between the hydrogen absorption and desorption branches.⁴⁸ In contrast, the isotherm measured with the fiber decorated with the Pd₇₅Au₂₅ alloy nanoparticle array exhibits the anticipated complete suppression of the hysteresis^{44,53} due to the reduced critical temperature of the phase transition by Au-atom induced lattice strain,⁶⁰ corroborating the homogeneous alloy formation.^{25,53} In this way, the sensing characteristics are greatly improved since accurate hydrogen detection with a wide dynamic range becomes available.⁵³

We also investigated the temporal response characteristics of the Pd and Pd₇₅Au₂₅ fiber-optic sensors upon hydrogen absorption to and desorption from 40 mbar hydrogen partial pressure (*i.e.* lower flammability limit), respectively, at 30 °C



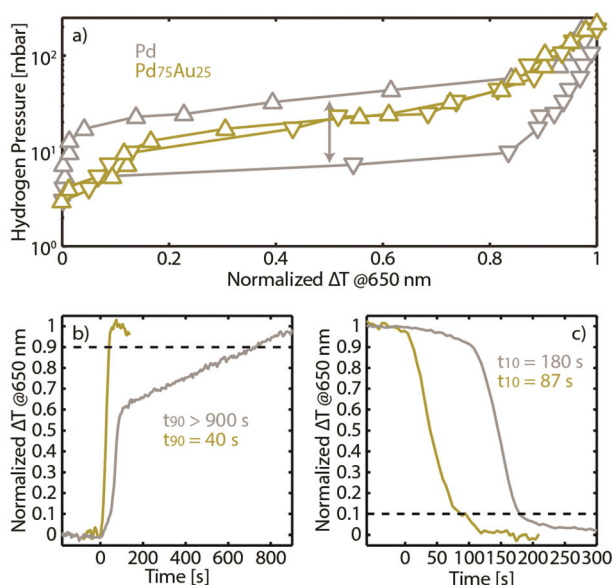


Fig. 4 (a) Optical pressure-composition isotherms of Pd and Pd₇₅Au₂₅ alloy nanoparticles measured directly on the fibers at 30 °C after pattern transfer. Up- and downward triangles denote the absorption and desorption branches of the isotherm, respectively. The arrow marks the hysteresis gap between absorption and desorption branches for pure Pd. Note the complete suppression of hysteresis in the alloy sensor. (b) Hydrogen absorption and (c) desorption temporal response of Pd and Pd₇₅Au₂₅ alloy fiber optic sensors to a stepwise H₂ partial pressure change from 0 to 40 mbar and *vice versa*. The dashed lines in panels (b) and (c) mark the 90% and 10% level of the total response, respectively. The distinct change in trend for the pure Pd can be attributed to different kinetics in the low concentration solid-solution regime (α -phase) and across the first order phase transition when the hydride (β -phase) is formed.

(Fig. 4b and c). Clearly, the Pd₇₅Au₂₅ sensor outperforms the neat Pd in both response (t_{90}) and recovery time (t_{10}). This general trend is in good agreement with previous reports of these two systems at the qualitative level (note also that the faster response compared to the data in Fig. 3 is due to a larger applied H₂ partial pressure difference). However, quantitatively, the response from both sensors is significantly slower than previously reported, where *e.g.* for Pd₇₅Au₂₅ a response

time of <5 s was achieved.⁵³ To explain this difference, we note that the experiment here was performed in a flow reactor with large volume⁶¹ and rather gradual partial pressure change (see Methods), in contrast to our previous study, which was done in a vacuum chamber that enables hydrogen pressure change at the sub-second timescale level.

Finally, we scrutinized the robustness of the transferred nanoparticles by exposing the Pd₇₅Au₂₅ fiber sensor to 110 cycles of 25% H₂ in synthetic air carrier gas, to mimic real application conditions. As shown in Fig. 5, even with oxygen in the feed, the sensor responds consistently and with the same amplitude to hydrogen during the entire ~20 h test. The slight change of baseline level that occurs at *ca.* 700 min we assign to a minute movement of the fiber. Since the sensor fiber is only loosely “clamped” into the bifurcator even the tiniest movement will slightly alter the amount of transmitted light and thus cause this artefact in our setup (see Methods). Nevertheless, the most important result here is that, despite the baseline shift, the overall response magnitude remains constant throughout the experiment in air.

Conclusions

In summary, we have demonstrated the successful deposition of arrays of tailored nanostructures made by nanofabrication, onto an optical fiber *via* pattern transfer. Specifically, we employed HCL to nanofabricate arrays of Au, Pd and Pd₇₅Au₂₅ alloy nanoparticles onto a flat parent support, which we then transferred onto the unclad tip of a commercial optical fiber to realize a hysteresis-free fiber-optic nanoplasmonic hydrogen sensor. We confirmed the functionality of the device by measuring its hydrogen sensing characteristics in response to different hydrogen partial pressures below the flammability limit of 4%, for which we find a linear correlation in good agreement with Sievert’s law for solid solutions. We also characterized the pressure-composition isotherms of an array of neat Pd and of Pd₇₅Au₂₅ alloy nanoparticles transferred onto optical fibers, and found all the anticipated characteristics of the two systems, such as the existence and suppression of hysteresis, respectively, to be retained. Analysis of the

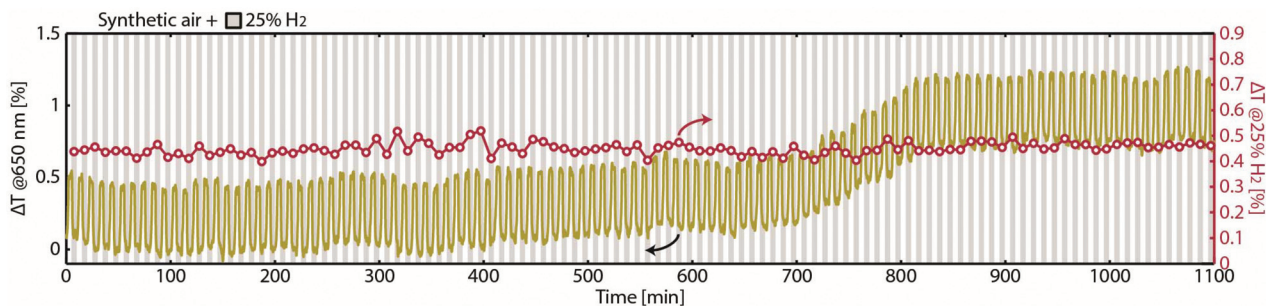


Fig. 5 ΔT response of Pd₇₅Au₂₅ alloy nanoparticles to 110 cycles of 25% H₂ in synthetic air. A small baseline shift occurs after *ca.* 700 min due to minuscule movement of the fiber. Nevertheless, a constant ΔT signal amplitude is observed throughout the entire experiment (red circles), demonstrating the excellent stability of the transferred nanoparticles and the reproducibility of their absolute response to hydrogen.



temporal response to increasing and decreasing hydrogen partial pressure in the fiber-optic sensors' environment also revealed a significantly shorter response time for the alloy sensor, in good agreement with earlier studies of the same systems in flat sensor designs. Finally, we demonstrated excellent stability of the transferred alloy nanoparticles, which operate consistently over 100 hydrogenation cycles in synthetic air.

In a wider perspective, our work opens the door to the integration of complex nanofabricated structures and their arrangements in tailored arrays with fiber optics to realize optical sensors, which we predict to find application in a wide range of disciplines, spanning from gas- and chemosensing to biosensing. The particular generic advantage that becomes available by our approach is that their sensitivity and optical fingerprint can be engineered and maximized by employing tailored nanostructures in terms of size, shape, arrangement and chemical composition,²⁶ which are readily available by nanofabrication tools that are only compatible with flat surfaces.

Conflicts of interest

There are no conflicts to declare.

Acknowledgements

We acknowledge financial support from the Knut and Alice Wallenberg Foundation project 2016.0210 and the Swedish Foundation for Strategic Research Framework project RMA15-0052. We also thank the Knut and Alice Wallenberg Foundation for their support of the infrastructure in the MC2 nanofabrication laboratory at Chalmers and acknowledge fruitful discussions with Kristof Lodewijks, Chatdanai Lumdee and Alexandre Dmitriev.

Notes and references

- 1 S. S. Yin and P. Ruffin, in *Wiley Encyclopedia of Biomedical Engineering*, John Wiley & Sons, Inc., Hoboken, NJ, USA, 2006.
- 2 B. A. Flusberg, E. D. Cocker, W. Piyawattanametha, J. C. Jung, E. L. M. Cheung and M. J. Schnitzer, *Nat. Methods*, 2005, **2**, 941–950.
- 3 A. Cobo, A. Q. Incera, J. M. López-Higuera and L. R. Cobo, *J. Lightwave Technol.*, 2011, **29**, 587–608.
- 4 Y. Zhang, H. Peng, X. Qian, Y. Zhang, G. An and Y. Zhao, *Sens. Actuators, B*, 2017, **244**, 393–416.
- 5 O. S. Wolfbeis, *Anal. Chem.*, 2008, **80**, 4269–4283.
- 6 M. Shortreed, R. Kopelman, M. Kuhn and B. Hoyland, *Anal. Chem.*, 1996, **68**, 1414–1418.
- 7 J. Homola, S. S. Yee and G. Gauglitz, *Sens. Actuators, B*, 1999, **54**, 3–15.
- 8 R. C. Jorgenson and S. S. Yee, *Sens. Actuators, B*, 1993, **12**, 213–220.
- 9 B. D. Gupta, in *Reviews in Plasmonics 2010*, ed. C. D. Geddes, Springer, New York, 2012, pp. 105–137.
- 10 K. M. Mayer and J. H. Hafner, *Chem. Rev.*, 2011, **111**, 3828–3857.
- 11 S. F. Cheng and L. K. Chau, *Anal. Chem.*, 2003, **75**, 16–21.
- 12 M. Wakao, S. Watanabe, Y. Kurahashi, T. Matsuo, M. Takeuchi, T. Ogawa, K. Suzuki, T. Yumino, T. Myogadani, A. Saito, K. Muta, M. Kimura, K. Kajikawa and Y. Suda, *Anal. Chem.*, 2017, **89**, 1086–1091.
- 13 T.-C. Chang, C.-C. Wu, S.-C. Wang, L.-K. Chau and W.-H. Hsieh, *Anal. Chem.*, 2013, **85**, 245–250.
- 14 C. Christopher, A. Subrahmanyam and V. V. R. Sai, *Plasmonics*, 2018, **13**, 493–502.
- 15 A. Hosoki, M. Nishiyama and K. Watanabe, *Appl. Opt.*, 2017, **56**, 6673.
- 16 J. Chen, S. Shi, R. Su, W. Qi, R. Huang, M. Wang, L. Wang and Z. He, *Sensors*, 2015, **15**, 12205–12217.
- 17 M. Grzelczak, J. Pérez-Juste, P. Mulvaney and L. M. Liz-Marzán, *Chem. Soc. Rev.*, 2008, **37**, 1783–1791.
- 18 C. J. Murphy, T. K. Sau, A. M. Gole, C. J. Orendorff, J. Gao, L. Gou, S. E. Hunyadi and T. Li, *J. Phys. Chem. B*, 2005, **109**, 13857–13870.
- 19 T. K. Sau and A. L. Rogach, *Adv. Mater.*, 2010, **22**, 1781–1804.
- 20 B. Ai, H. Möhwald, D. Wang and G. Zhang, *Adv. Mater. Interfaces*, 2017, **4**, 1600271.
- 21 C. L. Haynes and R. P. Van Duyne, *J. Phys. Chem. B*, 2001, **105**, 5599–5611.
- 22 H. Fredriksson, Y. Alaverdyan, A. Dmitriev, C. Langhammer, D. S. Sutherland, M. Zäch and B. Kasemo, *Adv. Mater.*, 2007, **19**, 4297–4302.
- 23 A. A. Tseng, K. Chen, C. D. Chen and K. J. Ma, *IEEE Trans. Electron. Packag. Manuf.*, 2003, **26**, 141–149.
- 24 K. Lodewijks, V. Miljkovic, I. Massiot, A. Mekonnen, R. Verre, E. Olsson and A. Dmitriev, *Sci. Rep.*, 2016, **6**, 28490.
- 25 F. A. A. Nugroho, B. Iandolo, J. B. Wagner and C. Langhammer, *ACS Nano*, 2016, **10**, 2871–2879.
- 26 F. A. A. Nugroho, I. Darmadi, V. P. Zhdanov and C. Langhammer, *ACS Nano*, 2018, **12**, 9903–9912.
- 27 M. Yang and J. Dai, *Photonic Sens.*, 2012, **2**, 14–28.
- 28 N. A. Isaac, P. Ngene, R. J. Westerwaal, J. Gaury, B. Dam, A. Schmidt-Ott and G. Biskos, *Sens. Actuators, B*, 2015, **221**, 290–296.
- 29 S. Sekimoto, H. Nakagawa, S. Okazaki, K. Fukuda, S. Asakura, T. Shigemori and S. Takahashi, *Sens. Actuators, B*, 2000, **66**, 142–145.
- 30 M. Tabib-Azar, B. Sutapun, R. Petrick and A. Kazemi, *Sens. Actuators, B*, 1999, **56**, 158–163.
- 31 M. Yang, H. Liu, D. Zhang and X. Tong, *Sens. Actuators, B*, 2010, **149**, 161–164.
- 32 M. A. Butler, *Sens. Actuators, B*, 1994, **22**, 155–163.
- 33 R. J. Westerwaal, S. Gersen, P. Ngene, H. Darmeveil, H. Schreuders, J. Middelkoop and B. Dam, *Sens. Actuators, B*, 2014, **199**, 127–132.



- 34 T. Mak, R. J. Westerwaal, M. Slaman, H. Schreuders, A. W. van Vugt, M. Victoria, C. Boelsma and B. Dam, *Sens. Actuators, B*, 2014, **190**, 982–989.
- 35 S. Tang, B. Zhang, Z. Li, J. Dai, G. Wang and M. Yang, *Opt. Express*, 2015, **23**, 22826.
- 36 B. Sutapun, M. Tabib-Azar and A. Kazemi, *Sens. Actuators, B*, 1999, **60**, 27–34.
- 37 J. Dai, M. Yang, Y. Chen, K. Cao, H. Liao and P. Zhang, *Opt. Express*, 2011, **19**, 6141.
- 38 J. Jiang, G.-M. Ma, C.-R. Li, H.-T. Song, Y.-T. Luo and H.-B. Wang, *IEEE Photonics Technol. Lett.*, 2015, **27**, 1453–1456.
- 39 Y. H. Kim, M. J. Kim, B. S. Rho, M.-S. Park, J.-H. Jang and B. H. Lee, *IEEE Sens. J.*, 2011, **11**, 1423–1426.
- 40 F. Gu, G. Wu and H. Zeng, *Nanoscale*, 2015, **7**, 924–929.
- 41 P. Tobiška, O. Hugon, A. Trouillet and H. Gagnaire, *Sens. Actuators, B*, 2001, **74**, 168–172.
- 42 R. Tabassum and B. D. Gupta, *J. Opt.*, 2016, **18**, 015004.
- 43 A. Hosoki, M. Nishiyama, H. Igawa, A. Seki, Y. Choi and K. Watanabe, *Sens. Actuators, B*, 2013, **185**, 53–58.
- 44 R. J. Westerwaal, J. S. A. Rooijmans, L. Leclercq, D. G. Gheorghe, T. Radeva, L. Mooij, T. Mak, L. Polak, M. Slaman, B. Dam and T. Rasing, *Int. J. Hydrogen Energy*, 2013, **38**, 4201–4212.
- 45 J. I. Avila, R. J. Matelon, R. Trabol, M. Favre, D. Lederman, U. G. Volkmann and A. L. Cabrera, *J. Appl. Phys.*, 2010, **107**, 023504.
- 46 F. D. Manchester, A. San-Martin and J. M. Pitre, *J. Phase Equilib.*, 1994, **15**, 62–83.
- 47 A. C. Switendick, *J. Less-Common Met.*, 1987, **130**, 249–259.
- 48 R. B. Schwarz and A. G. Khachatryan, *Acta Mater.*, 2006, **54**, 313–323.
- 49 C. Wadell, S. Syrenova and C. Langhammer, *ACS Nano*, 2014, **8**, 11925–11940.
- 50 V. Bérubé, G. Radtke, M. Dresselhaus and G. Chen, *Int. J. Energy Res.*, 2007, **31**, 637–663.
- 51 Z. Zhao, Y. Sevryugina, M. A. Carpenter, D. Welch and H. Xia, *Anal. Chem.*, 2004, **76**, 6321–6326.
- 52 M. Matuschek, D. P. Singh, H. H. Jeong, M. Nesterov, T. Weiss, P. Fischer, F. Neubrech and N. Liu, *Small*, 2018, **14**, 1702990.
- 53 C. Wadell, F. A. A. Nugroho, E. Lidström, B. Iandolo, J. B. Wagner and C. Langhammer, *Nano Lett.*, 2015, **15**, 3563–3570.
- 54 E. Lee, J. M. Lee, E. Lee, J.-S. Noh, J. H. Joe, B. Jung and W. Lee, *Thin Solid Films*, 2010, **519**, 880–884.
- 55 M. A. Poyli, V. M. Silkin, I. P. Chernov, P. M. Echenique, R. D. Muiño and J. Aizpurua, *J. Phys. Chem. Lett.*, 2012, **3**, 2556–2561.
- 56 I. Zorić, E. M. Larsson, B. Kasemo and C. Langhammer, *Adv. Mater.*, 2010, **22**, 4628–4633.
- 57 A. Remhof and A. Borgschulte, *ChemPhysChem*, 2008, **9**, 2440–2455.
- 58 F. A. A. Nugroho, C. Xu, N. Hedin and C. Langhammer, *Anal. Chem.*, 2015, **87**, 10161–10165.
- 59 P. Chen, N. T. Tran, X. Wen, Q. Xiong and B. Liedberg, *ACS Sens.*, 2017, **2**, 235–242.
- 60 S. Luo, D. Wang and T. B. Flanagan, *J. Phys. Chem. B*, 2010, **114**, 6117–6125.
- 61 F. A. A. Nugroho, A. Diaz de Zerio Mendaza, C. Lindqvist, T. J. Antosiewicz, C. Müller and C. Langhammer, *Anal. Chem.*, 2017, **89**, 2575–2582.

